

ANALYSIS OF A PHASE MODULATED INTERFEROMETRIC ELECTRO-OPTIC BPM AT THE CERN SPS

M. Z. C. Bosman*, S. M. Gibson, D. M. Harryman, A. Arteche
 John Adams Institute at Royal Holloway, University of London, UK
 T. Lefèvre, T. E. Levens, CERN, Geneva, Switzerland

Abstract

The Electro-Optic Beam Position Monitor (EO-BPM) is a new diagnostic tool being developed to enhance the intra-bunch transverse beam position monitoring in the High Luminosity LHC at CERN. This EO-BPM has been installed in the Super Proton Synchrotron (SPS) since 2024. The Pockels effect in lithium niobate crystals is exploited to detect the propagating electric field from passing proton bunches, enabling measurement of beam position and intra-bunch instabilities. Light is conveyed from a remote laser via optical fibres to a Mach-Zehnder interferometer formed between two waveguide pick-ups. The rapid response of the EO-BPM enables intra-bunch turn-by-turn measurements. Data recorded over a range of beam conditions have been studied to characterise its performance, stability, and sensitivity. This paper presents the latest data collected from the SPS and discusses the analysis and future development of the EO-BPM.

INTRODUCTION

The High-Luminosity Large Hadron Collider (HL-LHC) at CERN will increase the luminosity of the LHC by installing crab cavities to improve bunch overlap at the interaction point which require high-bandwidth diagnostics [1]. Electro-optical systems offer fast response and strong resistance to electrical noise, making them attractive for high-bandwidth beam position measurements in accelerator environments [2].

Working Principle

Lithium niobate (LN) is a birefringent electro-optic crystal [3], meaning that one of its three principal refractive indices differs from the others. Through the Pockels effect, this birefringence can be modulated by applying an external electric field. When linearly polarised laser light passes through the crystal, interferometric techniques can detect the resulting change in refractive index. This enables measurement of the external field, which in this context corresponds to the bunch shape [4].

The Electro-Optic Beam Position Monitor (EO-BPM) employs a fibre-coupled 780 nm laser, which is split, passing through two opposing LN crystals on either side of the beampipe (see Fig. 1). The laser then recombines to act as an Mach-Zehnder (MZ) interferometer. Since the refractive index of each crystal changes linearly with the applied electric field from the proton bunch, the response of this

interferometer is of the form:

$$V = A + B \cos \left(\phi_0 + \pi \frac{E}{E_\pi} \right), \quad (1)$$

where ϕ_0 is defined as the phase offset, E_π the electric field required for a phase advance of π and E is given by:

$$E = \begin{cases} E_l, & \text{for the left side mode interferometer} \\ E_r, & \text{for the right side mode interferometer} \\ E_l - E_r, & \text{for the difference interferometer} \end{cases}$$

with E_l and E_r being the fields in the left and right crystals, respectively [5].

Previous Iterations

The EO-BPM design has evolved since the initial installation in the SPS in 2016. From free space optics and low signal strength, to a fibre-coupled laser interferometer with several techniques to increase electric field modulation [5–8].

The main challenge cited in the 2024 proceedings was a mismatch of the pick-ups leading to a combination of sum and difference signals [5]. To address this, the new pick-up is adjustable and can be calibrated in situ. Additionally, a new phase control mechanism allows for three separate interferometric read-outs.

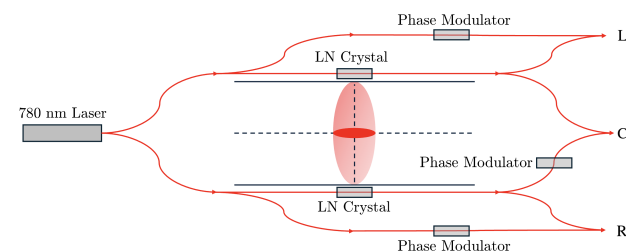


Figure 1: New EO-BPM splitter tree comprising of three Mach-Zehnder interferometers.

DESIGN OF ADJUSTABLE PICK-UP

Button Design

The new button changes several components. The conical design has been replaced by a cylindrical structure surrounded by ceramic, with a characteristic impedance of 20Ω , matching that of the bottom electrode.

* max.bosman@rhul.ac.uk

Figure 2 shows a longitudinal cross section of the pick-up. The bottom electrode (blue) is exposed to the inside of the beampipe. It is in contact with the LN crystal, which in turn is in contact with the top electrode.

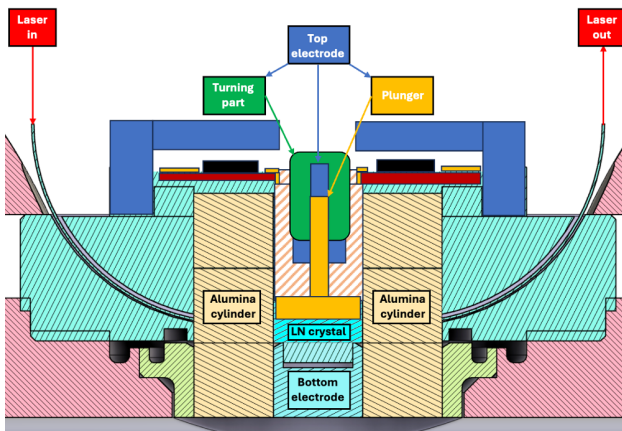


Figure 2: Longitudinal diagram of adjustable pick-up.

Differential Micrometer

The top electrode consists of three parts: a static copper outer part, a turnable brass middle part, and a vertically translating copper inner part. The inner part contains a plunger connected to a thin blade for focusing the beam field through the crystal. Its vertical translation affects the capacitive coupling with the bottom electrode and the LN crystal as dielectric medium.

The middle part consists of brass to prevent abrasion. It is threaded on the outside and tapped on the inside. The inner thread pitch is 0.25 mm while the outer is 0.275 mm. This ensures that every turn of the middle part moves the plunger 25 μm .

OPTICAL LAYOUT

The optical layout consists of a 100 mW 780 nm laser, split into four arms. These arms pass through either an LN crystal, a phase modulator, or both. The laser fibres are then recombined into three MZ interferometers: left (L), common (C), and right (R), see Fig. 1. This layout introduces an optical splitter tree with three phase modulators, guaranteeing a stable phase offset for all three read-outs.

Phase Stabilisation

The phase modulators allow for stabilisation of the phase offset from Eq. (1) in all three modes independently. The output from each of the three modes is passed through a 1 kHz low-pass filter to isolate the DC component. This DC signal is then sent to a feedback controller, which actively adjusts a bias voltage to maintain a fixed initial phase across each interferometer. This ensures the phase offset is kept around its desired value of $\frac{\pi}{2}$ [5, 9].

Figure 3 shows the phase offset for the three outputs taken over 2 minutes. The DC voltage was recorded and converted

to radians when the phase offset drifts freely, or when the phase is controlled. The measured phase offsets are: common: 1.57 ± 0.44 rad; left: 1.59 ± 0.37 rad; right: 1.56 ± 0.36 rad. Phase control has improved significantly from [5].

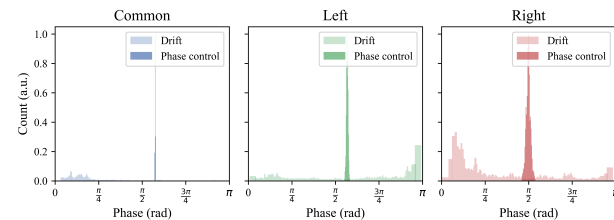


Figure 3: Histogram of phase offset phase modulated measurements and random drift.

ASSEMBLY AND INSTALLATION

Figure 4 shows the three parts of the differential micrometer, as well as parts of the ceramic cylinder. A slot is made in one of the ceramic parts to allow fibre holder components connected to the waveguide crystal to pass through. The ceramic parts are then stacked so that they make contact with the bottom electrode and ceramic seal on the beampipe, when the button is attached [5]. This electrode and ceramic feedthrough has a characteristic impedance of 20Ω . The cylinder design results in a button that is matched to 20Ω at the electrodes on either side of the crystal. The top electrode is terminated to a 20Ω load through a PCB.

The assembled button is shown in Fig. 5. Visible at the centre is the Allen key-shaped hole of the middle cylinder, which enables micron-level adjustment. The optical fibres are shown in blue. The retractable calibration wire is encased in a transparent sheath on the left. During in situ calibration, this wire is extended to electrically connect to the bottom electrode. During normal operation, it is retracted into the button housing. The frequency response of the adjustable button was tested using a Vector Network Analyser (VNA) to compare to the fixed button from [5].

A hollow cylindrical body with a ceramic washer and bottom electrode brazed into it was used to mount the button. A rod was placed inside the body, forming a coaxial line. Conical transitions were mounted onto either side of the coaxial

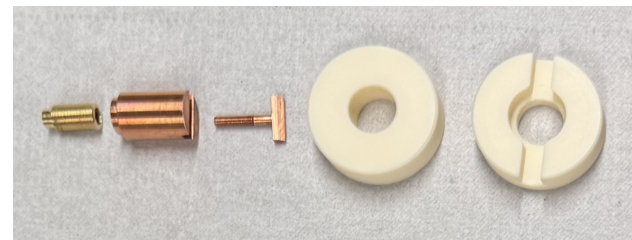


Figure 4: Five internal components of new EO-BPM button; from left to right: middle top electrode, outer top electrode, central top electrode and plunger, ceramic cylinder, ceramic cylinder with notch for fibre optics.

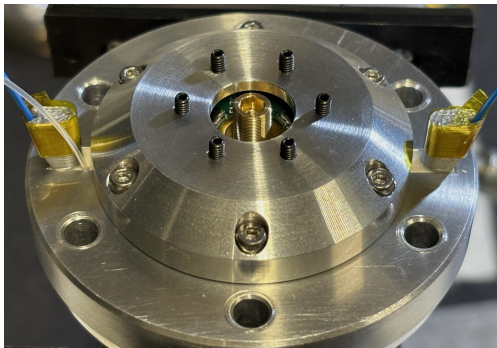


Figure 5: External view of assembled EO-BPM button, showing laser fibre entry and exit points, calibration wire and turnable top electrode part.

line, ending in SMA connectors. These SMA connectors were used to connect the VNA, which sends an excitation signal and records transmission. The transmission for both fixed and adjustable buttons is shown in Fig. 6. The new adjustable button exhibits a significantly lower resonance (at 2.42 GHz) than recorded on the fixed button (at 2.89 GHz). The new EO-BPM was installed in the CERN SPS during a technical stop in June 2025. The EO-BPM installation is shown in Fig. 7. The splitter tree is curled up and placed in fibre trays on top of the beampipe. Electrical control signals connect to the external phase modulators through three SMA cables on the left and right side. Optical fibres transmit the optical signal to and from the EO-BPM, shown on the bottom.

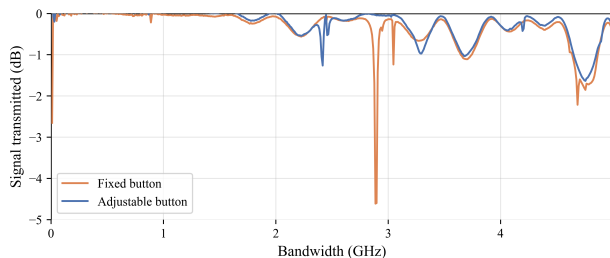


Figure 6: Vector Network Analyser comparison between fixed and adjustable button frequency response.

CALIBRATION

The new EO-BPM allows adjustment of the electrodes and signal calibration in the lab as well as in situ. These measurements were compared with simulated values for signal strength at different values of electrode displacement.

Electrode Displacement

The left button was adjusted in the lab to compare its signal output in response to displacement of the electrode. These values were compared to simulated values.

Simulations for the adjustable pick-up were performed in CST Studio Suite [10]. Amplitudes were recorded at different

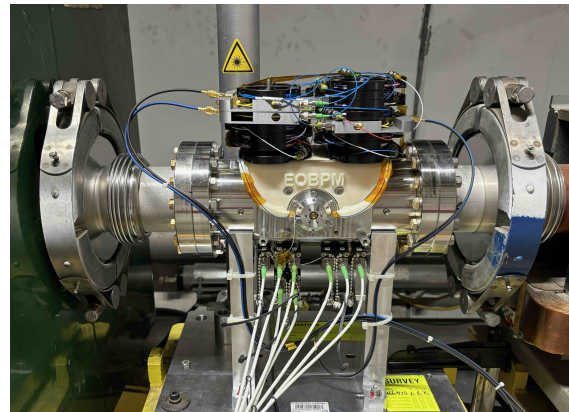


Figure 7: SPS beampipe portion with EO-BPM installed.

displacements and normalised at 0 µm displacement (plunger electrode touching the LN crystal).

To test the signal response from the EO-BPM, an interferometric setup like L from Fig. 1 was used. A 10 V step signal was injected into the bottom electrode, with the top electrode terminated at $20\ \Omega$. The top electrode was moved in 25 µm increments (one full rotation) from touching the LN crystal.

The normalised results of these measurements, as well as the simulated adjustable button, are shown in Fig. 8. As expected, both show a roughly reciprocal pattern. Interestingly, simulations show a peak signal with a non-zero displacement. This could be due to signal leaking through the sides of the crystal when the plunger is touching.

Note that there is no way to know for certain the proximity of the plunger electrode to the LN crystal, as the procedure provided only tactile cues, not visual.

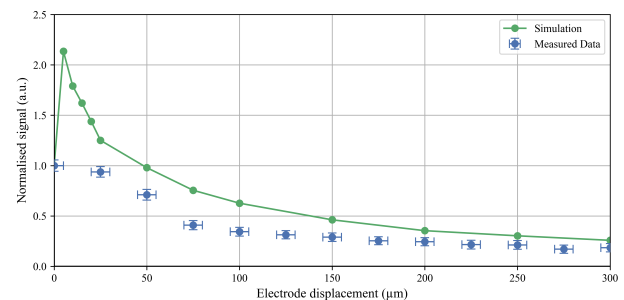


Figure 8: In lab calibration plot for electrode displacement: simulated adjustable button and measured single button.

A unique feature of this EO-BPM in relation to previous pick-ups is that it allows for in situ calibration. After both buttons were successfully mounted to the EO-BPM body, a calibration wire was extended to make electrical contact with the bottom electrode on both sides. The common mode interferometer (C) was measured with two sequentially injected signals: a 10 V ramp on the phase modulator ($V_\pi = 4\text{ V}$, corresponding to approximately 2.5π rotation) followed by a 10 V pulse directly on the calibration wires to the bottom

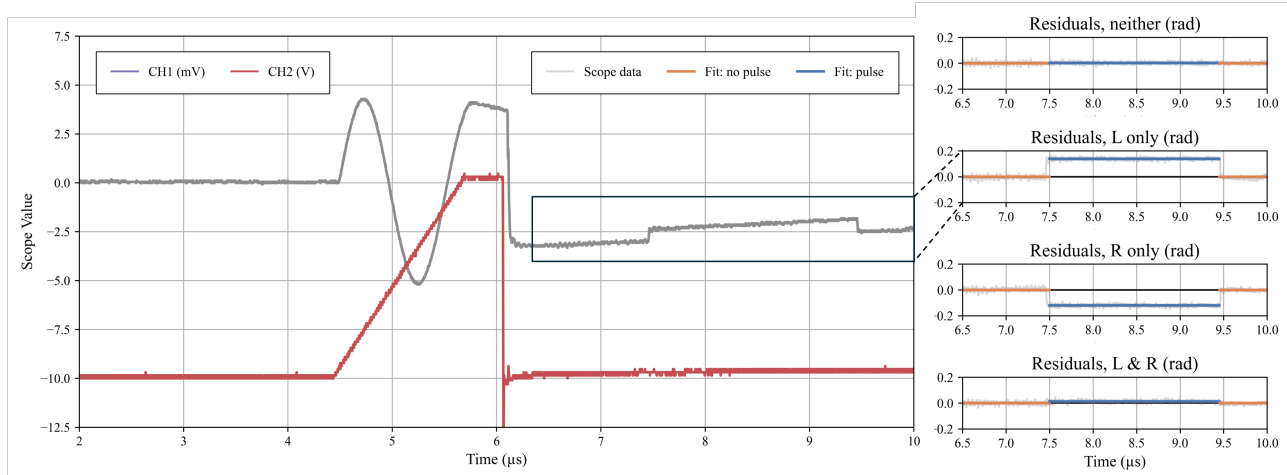


Figure 9: Left: oscilloscope output for calibration pulse; right: residual phase advance for all permutations of in situ calibration: neither side; left side; right side; both sides.

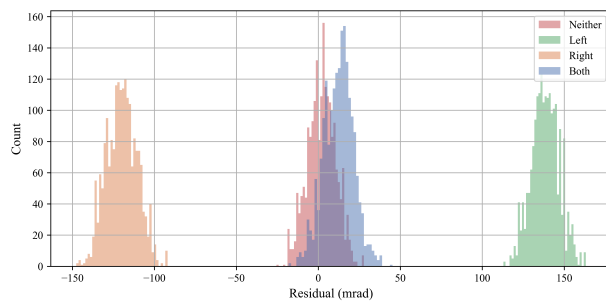


Figure 10: Histogram of residual phase advance for in situ oscilloscope calibration.

electrodes. The sine response from the ramp allows for conversion of the voltage signal into phase advance in radians. The top electrodes were adjusted until their signal responses were visually balanced.

Figure 9 shows the oscilloscope output for an injected signal on the left electrode, as well as residuals for the four permutations of the injected calibration pulse: neither (2.0 ± 12.1 mrad); left only (139 ± 12 mrad); right only (-120 ± 12 mrad); both (12.3 ± 12.1 mrad). The left button exhibits a somewhat stronger response, skewing the matching to the right.

All four figures consist of the common mode interferometer signal and 10 V ramp on top, as well as the common mode signal with two linear fits for the injected 10 V calibration pulse. Their results are represented as histograms in Fig. 10.

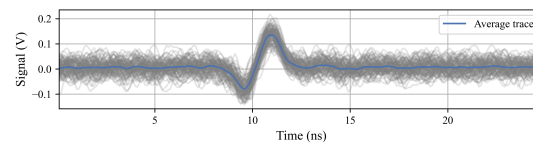
After calibration, the signal response of the common mode is approx. 10 % that of either side modes and within the noise level.

BEAM RESULTS

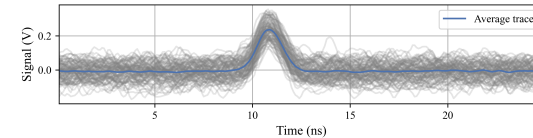
The balanced EO-BPM was exposed to HL-LHC type beam (2.3×10^{11} protons per bunch). The signal was recorded using a DXM12CF photodetector [11], a FEMTO HSA-

Y-1-60 amplifier [12] on a KeySight DSOS404A oscilloscope [13].

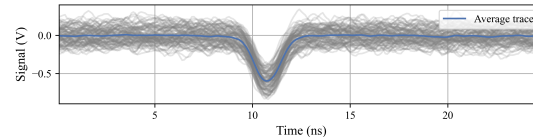
Figure 11 shows the EO-BPM response in common, left and right modes. 100 turns were recorded at injection (26 GeV) and averaged.



(a) Common mode.



(b) Left mode.



(c) Right mode.

Figure 11: Scope readout of EO-BPM at HiLumi-LHC type beam, single bunch averaged over 100 turns.

The signal-to-noise ratio (SNR) is 13 dB, 20 dB and 16 dB for common, left and right respectively. Several measurements were performed with beam at different horizontal displacements ranging from -8 mm to 6 mm. Figure 12 highlights 100 turn averaged oscilloscope plots of the common mode at -1 , 1 , 3 and 5 mm displacement from centre, at injection. These plots are consistent with a difference of two Gaussians at a 0.3 ns delay, likely due to the length difference between the phase modulator and patch fibre on the

arms of the common mode (see Fig. 1). To determine the system optical response, a time integral was performed over a 4.0 ns window around the averaged signal response. This signal is normalised to bunch charge and plotted against beam displacement in Fig. 13. The EO-BPM exhibits a clear linear response centred around 2.1 mm from beampipe centre. The direction of this offset is consistent with the in situ calibration shown in Fig. 9.

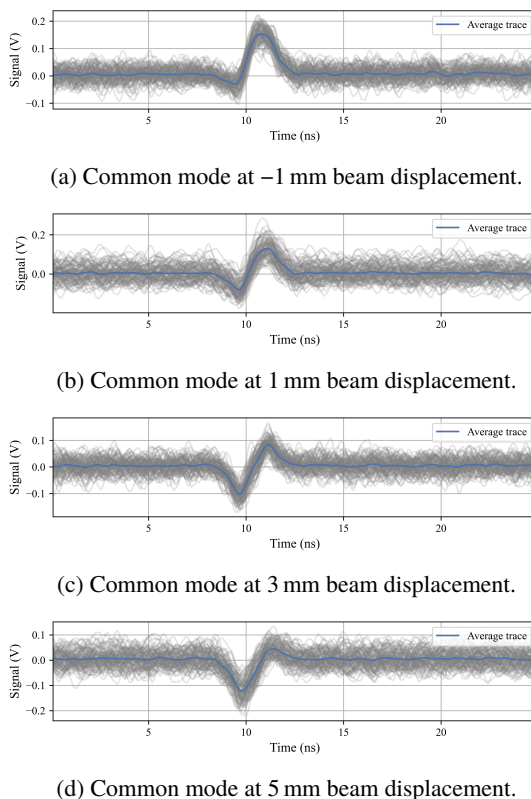


Figure 12: Scope readout of EO-BPM at HiLumi-LHC type beam common mode at different beam offset positions, single bunch averaged over 100 turns.

CONCLUSION AND OUTLOOK

An interferometric Electro-Optic Beam Position Monitor with adjustable electrodes and in situ calibration has been successfully installed and tested at the CERN SPS. The new design marks a step forward in adjustability, stable phase control, balancing common mode read-outs, and decreasing resonance. Initial beam measurements confirm its capability for individual bunch position monitoring.

Future work will address improving and tailoring signal strength to HL-LHC type beams. More precise matching of the buttons and of the optical arm length can centre the optical response of the common mode to provide accurate intra-bunch turn-by-turn data.

ACKNOWLEDGEMENTS

Work supported by UK STFC grants ST/N001583/1, ST/P00203X/1, Royal Holloway Univ. of London & CERN.

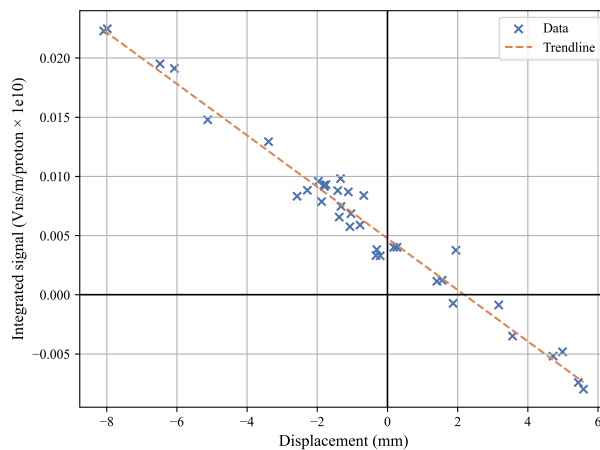


Figure 13: Integrated response of EO-BPM common mode, normalised to bunch charge, at different horizontal beam offset positions, showing a clear linear response 2.1 mm off-centre.

REFERENCES

- [1] O. Aberle *et al.*, *High-Luminosity Large Hadron Collider (HL-LHC): Technical design report*. Geneva, Switzerland: CERN, 2020. doi:[10.23731/CYRM-2020-0010](https://doi.org/10.23731/CYRM-2020-0010)
- [2] A. Schlägelhofer, “Remote sensing of fast beam signals using electro-optical modulators”, in *Proc. IBIC’24*, Beijing, China, Sep. 2024, pp. 219–223. doi:[10.18429/JACoW-IBIC2024-WEA12](https://doi.org/10.18429/JACoW-IBIC2024-WEA12)
- [3] R. S. Weis and T. K. Gaylord, “Lithium niobate: summary of physical properties and crystal structure”, *Appl. Phys. A*, vol. 37, no. 4, pp. 191–203, 1985. doi:[10.1007/BF00614817](https://doi.org/10.1007/BF00614817)
- [4] S. M. Gibson *et al.*, “High frequency electro-optic beam position monitors for intra-bunch diagnostics at the LHC”, in *Proc. IBIC’15*, Melbourne, Australia, Sep. 2015, pp. 606–610. doi:[10.18429/JACoW-IBIC2015-WEDLA02](https://doi.org/10.18429/JACoW-IBIC2015-WEDLA02)
- [5] M. Bosman *et al.*, “Design and deployment of an in-vacuum electro-optic BPM at the CERN SPS”, in *Proc. IBIC’24*, Beijing, China, Sep. 2024, pp. 161–165. doi:[10.18429/JACoW-IBIC2024-TUP46](https://doi.org/10.18429/JACoW-IBIC2024-TUP46)
- [6] A. Arteche *et al.*, “First beam tests at the CERN SPS of an electro-optic beam position monitor for the HL-LHC”, in *Proc. IBIC’17*, Grand Rapids, MI, USA, Aug. 2017, pp. 270–273. doi:[10.18429/JACoW-IBIC2017-TUPCF23](https://doi.org/10.18429/JACoW-IBIC2017-TUPCF23)
- [7] A. Arteche *et al.*, “Beam measurements at the CERN SPS using interferometric electro-optic pickups”, in *Proc. IBIC’19*, Malmö, Sweden, Sep. 2019, pp. 457–460. doi:[10.18429/JACoW-IBIC2019-WEA004](https://doi.org/10.18429/JACoW-IBIC2019-WEA004)
- [8] A. Arteche, S. M. Gibson, *et al.*, “Electro-optical BPM development for high luminosity LHC”, in *Proc. IBIC’22*, Kraków, Poland, Sep. 2022, pp. 181–185. doi:[10.18429/JACoW-IBIC2022-TU1I1](https://doi.org/10.18429/JACoW-IBIC2022-TU1I1)
- [9] D. Harryman *et al.*, “Investigation of read-out methods for electro-optical beam position monitor pickups”, presented at IBIC’25, Liverpool, UK, Sep. 2025, paper WEPMO26, this conference.

- [10] *CST Studio Suite 2024*, Dassault Systèmes, 2024. <https://www.3ds.com/products-services/simulia/products/cst-studio-suite/>
- [11] *DXM12CF ultrafast detector—spec sheet*, Thorlabs Inc., Ann Arbor, MI, USA, Aug. 2018. <https://www.thorlabs.com/drawings/1584d1892340daae-6AB24806-CDA7-5ECE-A0660D8871A241E3/DXM12CF-SpecSheet.pdf>
- [12] *HSA-Y-1-60 1 GHz high-speed amplifier datasheet*, FEMTO Messtechnik GmbH, Berlin, Germany, Sep. 2024. <https://www.femto.de/images/pdf-dokumente/de-hsa-y-1-60.pdf>
- [13] *Infinium S-Series Oscilloscopes data sheet (5991-3904)*, Keysight Technologies, Inc., Santa Rosa, CA, USA, May 2019. <https://www.keysight.com/us/en/assets/7018-04261/data-sheets/5991-3904.pdf>